# Baroclinic Instability of a Rotating Hadley Cell

BASIL N. ANTAR

*The University of Tennessee Space Institute, Tullahoma 37388*

WILLIAM W. FOWLIS

*Space Sciences Laboratory, Marshall Space Flight Center, Alabama 35812*

(Manuscript received 2 February 1981, in final form 12 May 1981)

ABSTRACT

The stability of a thin fluid layer between two rotating plates which are subjected to a horizontal temperature gradient is studied. First, the solution for the stationary basic state is obtained in a closed form. This solution identifies Ekman and thermal layers adjacent to the plates and interior temperature and velocity fields which are almost linear functions of height. Then the stability of that basic state with respect to infinitesimal zonal waves is analyzed via the solution of the complete viscous linear equations for the perturbations. The character of the growth rates is found to be similar to the growth rates of the classical baroclinic waves. The neutral stability curves for these waves possessed a knee in the Rossby-Taylor number plane to the left of which all perturbations are stable. The region of instability is found to depend on the Prandtl number, the vertical stratification parameter, and both the meridional and zonal wavenumbers. It is found in general that the flow is unstable for small enough Ekman numbers and for Rossby numbers less than 10. It is also found that increased vertical stable stratification and increased Prandtl number stabilize the flow.

## 1. Introduction

The mechanism of baroclinic instability has been the subject of much experimental and theoretical study during the past few decades. Its relevance to synoptic-scale atmospheric circulation and other geophysical phenomena has been recognized by meteorologists and geophysicists ever since the pioneering works of Charney (1947) and Eady (1949).

Baroclinic instability has been extensively studied in the laboratory for rotating flows in the cylindrical dishpan experiments of Fultz (1953), and the cylindrical annulus experiments of Hide (1958), Fultz *et al.* (1959), and Fowlis and Hide (1965). These experiments have shown that the symmetric zonal flow regime (Hadley regime) gives way to the asymmetric wave regime (Rossby regime) for certain ranges of values of the imposed conditions. These studies established diagrams known as the regime diagrams, similar to the one shown in Fig. 1, which consist of curves in the Rossby-Taylor number plane separating regions of symmetric flow from asymmetric flow.

There has been considerable effort at establishing regime diagrams, similar to Fig. 1, from stability analyses of simple viscous symmetric zonal flows. Lorenz's (1962) analysis, which was not strictly a stability analysis, treated simultaneously the basic state and the wave regime. However, in the process of simplifying the governing equations, to make them amenable for analytical solution, he restricted the shape of the flow pattern and introduced simplifying assumptions on the heating and friction laws. Although these assumptions precluded any quantitative comparison with experiments, his regime diagrams have the proper shape.

Barcilon (1964) established regime diagrams through the stability analysis of a simplified postulated basic state. By using linear functions in the interior of the fluid for the basic state, he was able to obtain closed form solutions for the perturbation equations through an asymptotic analysis. His analysis reduced the governing equations of the problem to essentially the inviscid baroclinic stability equations of Eady (1949) with modified boundary conditions. The viscous effects were incorporated in the boundary conditions through the Ekman compatibility conditions (Greenspan, 1968). The regime diagrams obtained by Barcilon are in good qualitative agreement with the annulus experimental results.

Numerous other studies on baroclinic instability have appeared since the work of Barcilon which incorporated additional effects to his original model. However, most of these studies relied on a postulated basic state and used the Ekman compatibility conditions for the viscous effects. O'Neil (1969),

0022-4928/81/102130-12$07.00

for instance, used a systematic asymptotic analysis to extend the work of Barcilon to account for the effects of sidewalls on the stability results and also to allow for a free upper surface. O'Neil's analysis produced regime diagrams which were almost identical to Barcilon's for a rigid upper lid and diagrams which were shifted to the left in the parameter plane for a free upper surface. An excellent summary of the various baroclinic stability results and their comparison with the annulus experiments may be found in the work of Kaiser (1970). Recently, Geisler and Fowlis (1979) extended the work of Barcilon to include latitudinal curvature effects through the $\beta$ plane. Their results give regime diagrams which are shifted still further to the left in the parameter plane.

In the present work we present a systematic stability analysis for the onset of baroclinic waves in a thin rotating fluid layer. Although the model used here has a similar geometrical configuration to the baroclinic stability studies cited above, the analysis differs in two essential ways from these studies. The analysis is systematic in that we do not postulate a basic state but obtain it through the solution of the full nonlinear governing equations of motion. The basic state obtained includes both the interior region and the Ekman and thermal layers adjacent to the planes. This solution for the basic state is obtained in an analytic closed form. Then the stability of that basic state with respect to small perturbations is investigated through the solution of the full viscous perturbation equations. Due to the complexity of the governing equations the stability results are obtained through numerical means. The analysis presented here follows the work of Hart (1972) on the stability of a thin nonrotating fluid layer with horizontal temperature gradients.

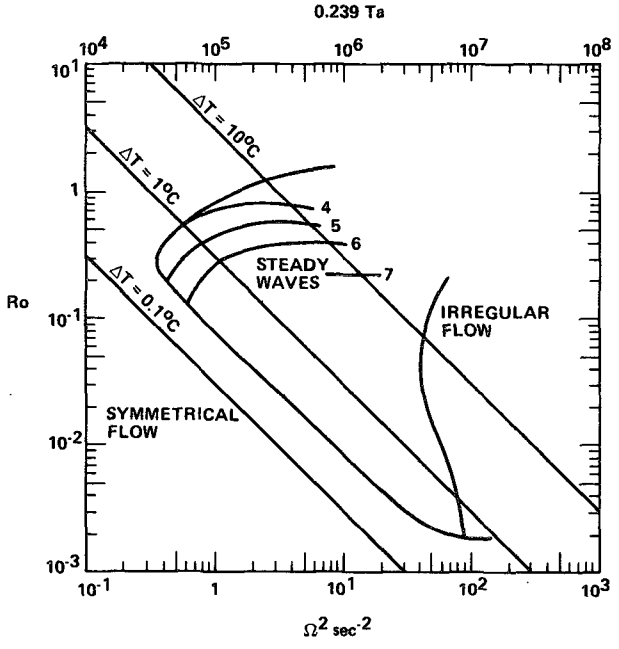


FIG. 1. Adaptation of the experimental regime diagram from Fowlis and Hide (1965) for the cylindrical annulus flows in which the boundary separates symmetrical flow from wave-like flow.

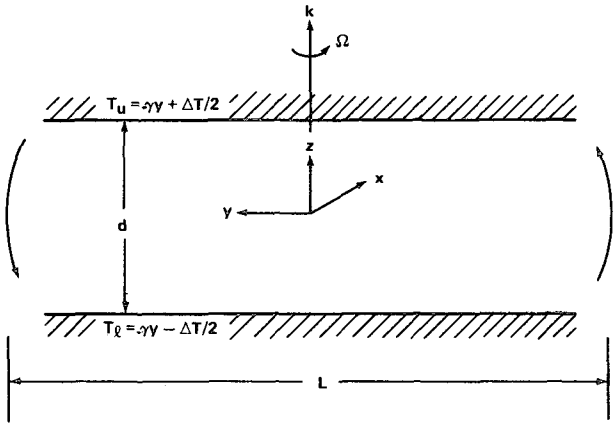


FIG. 2. A sketch of the geometry of the model and the coordinates.

The formulation of the theoretical model and the derivation of the basic state for the model are presented in Section 2. In Section 3 we present the derivation of the perturbation equations for the stability analysis of the basic state. In Section 4 a brief outline is presented of the numerical technique employed for the solution of the perturbation equations. Section 5 contains a discussion of the results and comparison with relevant previous work. Finally, pertinent conclusions regarding this work are discussed in Section 6.

## 2. The basic state

Since this study is concerned with stability analysis, the first step is to determine a stationary basic state whose stability is under investigation. We consider a Boussinesq fluid confined between two horizontal plates which are at a distance $d$ apart. The plates are assumed to extent to infinity in the $x$ direction and to very large distances in the $y$ direction. The coordinate system used is rectangular Cartesian with axes $(x, y, z)$ corresponding to the eastward, northward and vertical directions, respectively, and with the origin midway between the plates. The plates and the fluid layer are taken to rotate as a whole about the vertical axis with a constant angular velocity $\Omega$. In this model the plates are kept at a temperature which decreases linearly in the $y$ direction. To insure that the fluid is stably stratified in the interior, the temperature of the upper plate is kept uniformly at a higher temperature than the lower plate by an amount of $\Delta T$. A sketch of the model is shown in Fig. 2.

The governing equations for this model are the

momentum, energy and mass conservation equations, which take the following form in a rotating reference frame:

$$\frac{\partial \mathbf{V}}{\partial t} + \mathrm{Ro}\mathbf{V}\cdot\nabla\mathbf{V} + 2\mathbf{k}\times\mathbf{V} = -\nabla p + \mathrm{E}\nabla^2\mathbf{V} + \mathbf{k}T, \quad (1)$$

$$\sigma\frac{\partial T}{\partial t} + \sigma\,\mathrm{Ro}\mathbf{V}\cdot\nabla T = \mathrm{E}\nabla^2 T, \quad (2)$$

$$\nabla\cdot\mathbf{V} = 0, \quad (3)$$

where $\mathbf{V}$ is the velocity vector $(U, V, W)$ and

$$\mathrm{Ro} = \alpha g\gamma/\Omega^2,$$
$$\mathrm{E} = \nu/d^2\Omega,$$
$$\sigma = \nu/\kappa$$

are a thermal Rossby number, the Ekman number and the Prandtl number, respectively. The variables in Eqs. (1)–(3) have been made dimensionless by using $d$, $\Omega^{-1}$, $U_0$ and $\gamma d$ for the length, time, velocity and temperature scales, respectively. $U_0$ is the thermal wind which is defined by $\alpha g d\gamma/\Omega$, and $\gamma$ is the imposed horizontal temperature gradient at the boundaries, which is taken as a constant.

For the basic state we seek the stationary solutions to Eqs. (1)–(3) under the following assumptions. First, it is assumed that the flow field is two-dimensional in character. Second, it is assumed that the magnitude of the vertical velocity component $W$ is negligible in comparison with the other two components everywhere in the region of interest, i.e., $W = 0$ everywhere. Physically, this assumption amounts to restricting the flow field to a region sufficiently removed from vertical walls at $y = \pm L/2$. It should be understood, however, that in order to conserve mass the fluid should recirculate in such a way that it flows up one wall and down the other, always keeping the flow field in the region of interest unaffected by this motion. Although this assumption restricts the applicability of this model to only a few laboratory experiments, it has been shown (e.g., Williams, 1967) that in the stratified annulus flows with a rigid upper lid most of the vertical motion is indeed restricted to narrow boundary layers along the sidewalls. Such a flow may be approximated in the laboratory in a rotating cylindrical annulus with imposed temperature gradients along the horizontal boundaries. Under these restrictions Eqs. (1)–(3) take the forms

$$-2V = \mathrm{E}\partial^2 U/\partial z^2, \quad (4)$$

$$2U = \mathrm{E}\partial^2 V/\partial z^2 - \partial P/\partial y, \quad (5)$$

$$\sigma\,\mathrm{Ro}V\partial T/\partial y = \mathrm{E}\partial^2 T/\partial z^2, \quad (6)$$

$$T = \partial P/\partial z. \quad (7)$$

The above system of equations has been derived with the further restriction that the horizontal temperature gradient is constant everywhere in the interior of the fluid.

Next, we seek a solution for the system (4)–(7) subject to the following boundary conditions: the no-slip condition on the velocity at the plates, i.e.,

$$U = V = W = 0, \quad \text{at} \quad z = \pm\tfrac{1}{2}, \quad (8a)$$

and a conducting thermal boundary condition at the plates, i.e.,

$$T = \pm\Delta T/2 - y, \quad \text{at} \quad z = \pm\tfrac{1}{2}. \quad (8b)$$

The solution for the system (4)–(7) with these boundary conditions takes the form

$$U(z) = z/2 - f(z)/8, \quad (9)$$

$$V(z) = g(z)/8, \quad (10)$$

$$T(y, z) = -y + z\Delta T + \sigma\,\mathrm{Ro}[2z - f(z)]/8, \quad (11)$$

where

$$\left.\begin{aligned} f(z) &= [\cosh R(z+\tfrac{1}{2})\cos R(z-\tfrac{1}{2}) \\ &\quad - \cosh R(z-\tfrac{1}{2})\cos R(z+\tfrac{1}{2})]/h(R) \\ g(z) &= [\sinh R(z+\tfrac{1}{2})\sin R(z-\tfrac{1}{2}) \\ &\quad - \sinh R(z-\tfrac{1}{2})\sin R(z+\tfrac{1}{2})]/h(R) \\ h(R) &= \sinh^2(\tfrac{1}{2}R) + \sin^2(\tfrac{1}{2}R) \\ R &= E^{-1/2} \end{aligned}\right\}. \quad (12)$$

It can be seen from expression (11) for the basic state temperature field that the temperature may become very large for negative $y$. This is due to the basic assumption that the fluid is infinite in the $y$ direction. However, since physically the temperature at the plate should never exceed the maximum temperature in the fluid at $y = 0$, a limit on the application of the model may be obtained. Thus, the model must break down if

$$|T(0, z)|_{\max} \geq \Delta T + L/2d.$$

The evaluation of this expression will then give an upper limit on the value of $L/d$ for which the model is valid.

### 3. Perturbation equations

To investigate the stability of the basic state derived above, the field variables in (1)–(3) are first decomposed into a basic state and a perturbation component such that

$$\mathbf{V}^* = \mathbf{V}(z) + \mathbf{v}(x, y, z; t),$$
$$P^* = P(y, z) + p(x, y, z; t),$$
$$T^* = T(y, z) + \theta(x, y, z; t).$$

After substituting these variables into the governing equations (1)–(3) and subtracting the basic state,

equations governing the perturbation functions are obtained. For the stability analysis discussed in this work the perturbation equations are linearized, resulting in the following set of equations for the perturbation functions:

$$\frac{\partial \mathbf{v}}{\partial t} + \mathrm{Ro}\left(U\frac{\partial \mathbf{v}}{\partial x} + V\frac{\partial \mathbf{v}}{\partial y} + w\frac{\partial \mathbf{V}}{\partial z}\right) + 2\mathbf{k}\times\mathbf{v} = -\nabla p + \mathrm{E}\nabla^2\mathbf{v} + \mathbf{k}\theta, \quad (13)$$

$$\sigma\frac{\partial \theta}{\partial t} + \sigma\,\mathrm{Ro}\left(U\frac{\partial \theta}{\partial x} + V\frac{\partial \theta}{\partial y} + v\frac{\partial T}{\partial y} + w\frac{\partial T}{dz}\right) = \mathrm{E}\nabla^2\theta, \quad (14)$$

$$\nabla\cdot\mathbf{v} = 0. \quad (15)$$

Since Eqs. (13)–(15) are linear with coefficients which are independent of $x$, $y$ and $t$, they admit a separable solution of the form

$$f(x, y, z; t) = f(z)\exp[i(kx + ly - \omega t)]. \quad (16)$$

The solution form (16) may be characterized physically by a traveling oblique wave with wavenumber components $k$ and $l$ in the $x$ and $y$ directions, respectively, and whose frequency is $\omega$.

It is in general difficult to determine *a priori* which value of $l/k$ renders the perturbations most unstable. However, after solving the system (13)–(15) for a number of values of $l/k$, it was concluded that $l/k = 0$ represents the most unstable perturbation. This result will be discussed further in Section 5. Hence, since the two-dimensional, or purely zonal, perturbations seem to be the most unstable for a given set of parameters, the stability analysis to be presented here will be mainly concerned with these perturbations. For the two-dimensional case the perturbation functions may be written in the form

$$f(x, y, z; t) = f(z)\exp[ik(x - ct)], \quad (17)$$

where now $c$ is the wave speed and $k$ is the wavenumber in the zonal direction. Substituting (17) into (13)–(15) and eliminating the pressure from the momentum equations, the following system of ordinary differential equations governing the amplitude functions $v(z)$, $w(z)$ and $\theta(z)$ results:

$$\mathrm{E}(D^2 - k^2)^2 w + ik[(c - \mathrm{Ro}U)(D^2 - k^2)w + \mathrm{Ro}wD^2U + 2Dv] - k^2\theta = 0, \quad (18)$$

$$\mathrm{E}(D^2 - k^2)v + ik(c - \mathrm{Ro}U)v - \mathrm{Ro}wDV + 2iDw/k = 0, \quad (19)$$

$$\mathrm{E}(D^2 - k^2)\theta + ik\sigma(c - \mathrm{Ro}U)\theta - \sigma\,\mathrm{Ro}(v + wDT) = 0, \quad (20)$$

$$iku + Dw = 0, \quad (21)$$

where $D = d/dz$ is the differential operator.

Note that Eqs. (18)–(20) could have been simplified further to give a single eighth-order differential equation in terms of any of $u$, $v$, $w$ or $\theta$. However, for the specific numerical technique employed here, which will be discussed in Section 4, no advantage could be gained by such a simplification.

These perturbation equations are to be solved subject to the following boundary conditions

$$v = w = Dw = \theta = 0, \quad \text{at} \quad z = \pm\tfrac{1}{2}. \quad (22)$$

Since these conditions and the amplitude equations are homogeneous, it is clear that the total system constitutes an eigenvalue problem. Also, since the system is complex, any two real parameters may be considered as the eigenvalues. In the present case $k$ will be taken as real, while $c$ is complex, i.e.,

$$c = c_r + ic_i.$$

Thus the wave speed $c$ is the eigenvalue of the problem, while $u$, $v$, $w$ are the velocity eigenfunctions and $\theta$ is the temperature eigenfunction. The stability question is settled through the sign of $c_i$; if it is negative, then the system is stable, while if it is positive it is unstable.

At this point it is appropriate to present the perturbation equations for the three-dimensional disturbance case since use will be made of these equations to verify the conjecture concerning the most unstable perturbations. Thus, for future reference these equations are

$$i[\omega - \mathrm{Ro}(kU - lV)]\nabla^2 w + i\,\mathrm{Ro}w(kD^2V + lD^2U) + 2i(kDv - lDu) = -\mathrm{E}\nabla^4 w + m^2\theta, \quad (23)$$

$$i[\omega - \mathrm{Ro}(kU - lV)](m^2 v - ilDw) - \mathrm{Ro}kw(kDV - lDU) + 2ikDw = -\mathrm{E}\nabla^2(m^2 v - ilDw), \quad (24)$$

$$i[\omega - \mathrm{Ro}(kU - lV)]\theta + \sigma\,\mathrm{Ro}(v + wDT) = -\mathrm{E}\nabla^2\theta, \quad (25)$$

$$ku + lv - iDw = 0, \quad (26)$$

where

$$\nabla^2 = D^2 - m^2,$$

$$m^2 = k^2 + l^2.$$

The boundary conditions for these equations are the same as for the two-dimensional perturbations, i.e., (22).

It should be mentioned here that the quasi-geostrophic equations which are commonly used in baroclinic stability analyses may be obtained from (18)–(20) by neglecting the viscous terms and retaining only the first-order terms in the Rossby number (see Pedlosky, 1979). Thus, the analysis presented here through the solution of the full linearized perturbation equations will identify all of the baro-

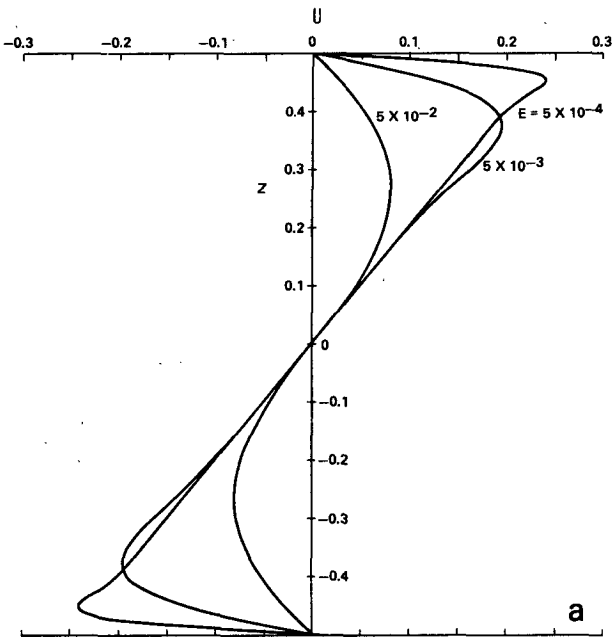


FIG. 3a. Zonal velocity component $U$ at three values of the Ekman number.

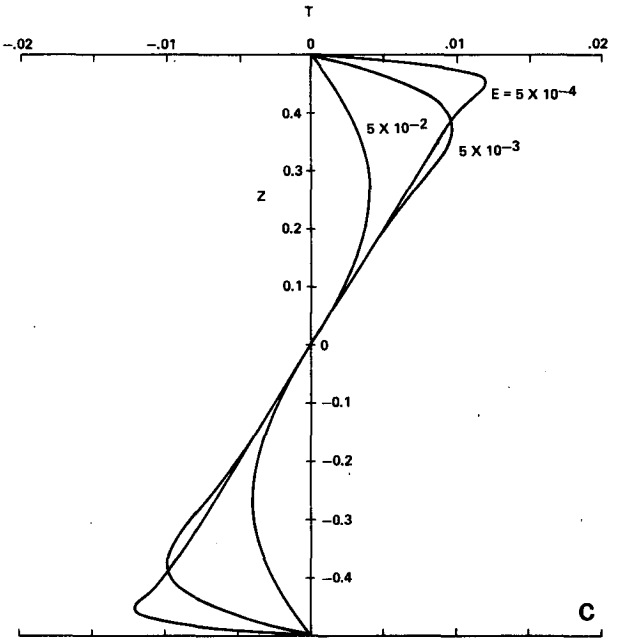


FIG. 3c. Temperature profile at $y = 0$ for $\sigma = 1$, Ro = 1 and $\Delta T = 0$.

clinic modes that are present in the flow field. However, in this study attention will be confined to only those baroclinic modes that exist for large Richardson numbers (see Stone, 1966).

## 4. The numerical technique

Since the governing differential equations, (18)–(21) and (23)–(26), form a linear eigenvalue problem for each system, a nontrivial solution should, in theory at least, be readily available. However, due to the complexity of the coefficients of these equations (the basic state), a closed form solution is out of the question. Thus, the only recourse at our disposal for solving these problems is through numerical means.

There are basically two direct methods for the numerical solution of ordinary differential eigenvalue problems. These are the matrix and the shooting methods. For a detailed review of both of these methods and the merits of using each see Davey (1978). Due to the complexity of both systems (each comprises an eighth-order coupled set), the shooting method is more suitable for the present problem. However, due to a certain peculiarity of the present problem the normal shooting technique will fail if implemented without any modifications. A failure will occur whenever a linear system contains either a very large or a very small parameter, multiplying the highest derivatives. Unfortunately, this is the situation in the present problem. For both of the systems considered here the Ekman number, E, always multiplies the highest derivatives in the equations. For baroclinic stability problems of interest, the Ekman number is usually less than $10^{-2}$ and often as low as $10^{-6}$. This difficulty may be overcome, through the orthonormalization of the linearly independent solutions at certain points in the range of integration. In all of the numerical solutions that are discussed in the next section the orthonormalization technique due to Conte (1966) is used.

To solve each of the eigenvalue problems a computer code was written with an eighth-order variable

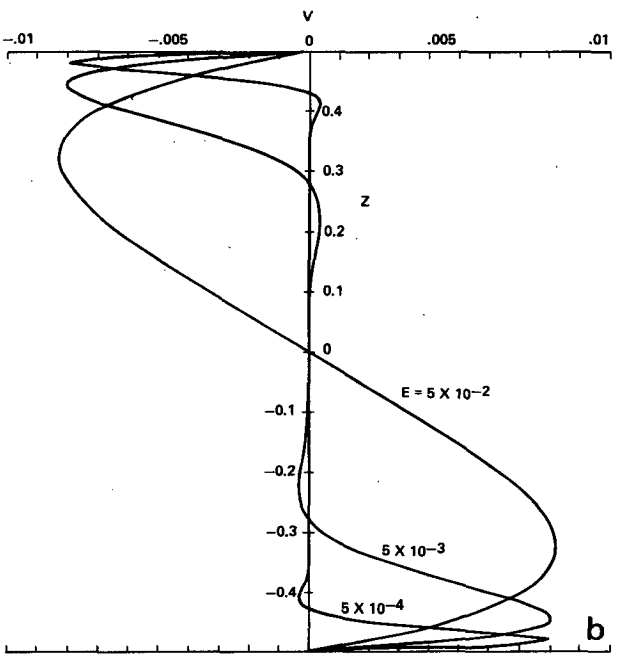


FIG. 3b. Meridional velocity component $V$.

step Runge-Kutta-Fehlberg initial value integrator (see Fehlberg, 1969). For the iteration procedure a Newton-Raphson method was used and the orthonormalization process was implemented at each integration step. All of the eigenvalues which are presented in the next section were produced with a relative tolerance of $10^{-4}$ in the iteration process (i.e., all eigenvalues presented are correct to within four significant figures). Also, due to the fact that at small Ekman numbers the Ekman layers on the plates are thin, the code was made to use at least 10 integration steps within each Ekman layer to ensure adequate resolution of these layers. Normally, if no convergence was achieved on the eigenvalues after 20 iterations, a different initial guess for the eigenvalue was used. However, if the initial guess was good a convergence was achieved after only a few iterations.

## 5. Results and discussion

### *a. The basic state*

The solution to the equations of motion for the stationary basic state is given by expressions (9)–(12) for both the meridional $V(z)$ and the zonal $U(z)$ velocity components, and for the temperature $T(z)$. It is clear from these solutions that, under the assumptions used, the velocity field is a function of the Ekman number E alone, while the temperature is a function of the Rossby number Ro, the Prandtl number $\sigma$ and the imposed vertical temperature difference $\Delta T$, as well as the Ekman number. Fig. 3 shows typical velocity and temperature profiles at $y = 0$ for a range of Ekman numbers.

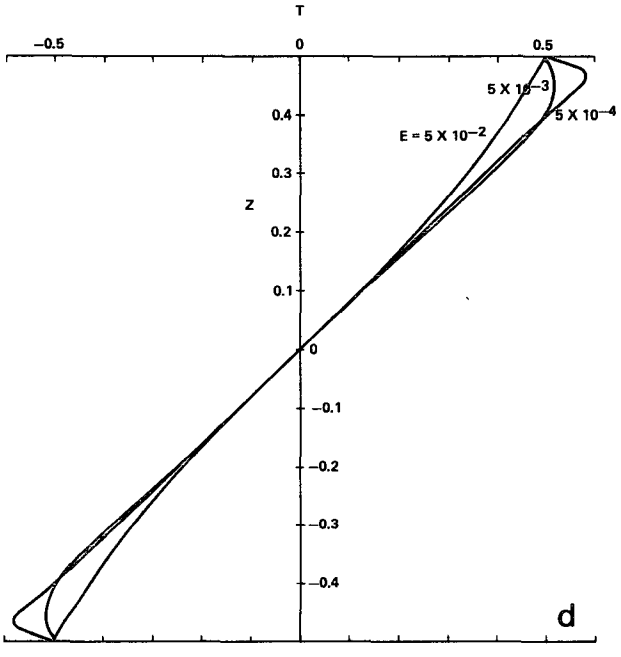


FIG. 3d. As in Fig. 3c for $\Delta T = 1$.

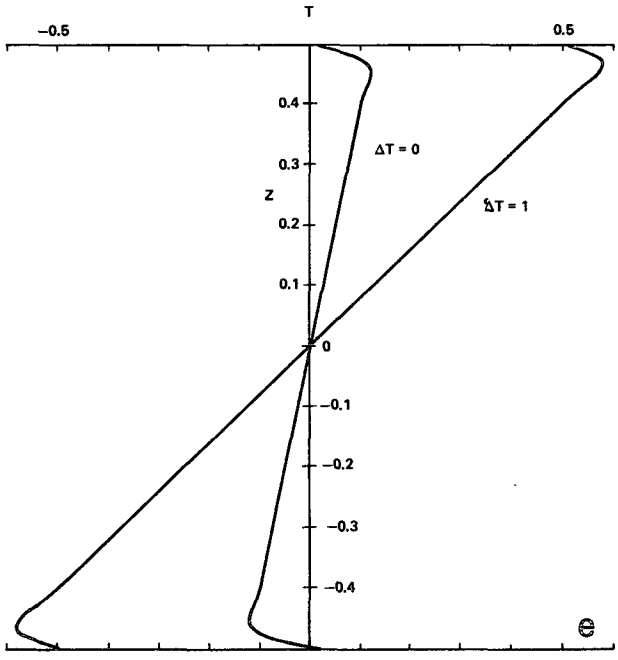


FIG. 3e. Temperature profiles at $y = 0$, $\sigma = 1$, Ro = 1 and E = $10^{-3}$ and $\Delta T = 0$ and 1.

It can be seen from Fig. 3a, for the zonal velocity component that there exist strong Ekman layers adjacent to the boundary plates with an almost linear variation over most of the interior region of the fluid for small Ekman numbers. It also can be seen that the effect of the Ekman number on the velocity field is almost insignificant in the interior when the Ekman number is less than $10^{-3}$. Also, it appears from inspecting Fig. 3a that the zonal velocity gradient $dU/dz$, in the interior of the fluid is almost constant regardless of the Ekman number. However, it is also clear that the strength of the zonal velocity field is the Ekman layers and the thickness of these layers is highly dependent on the Ekman number.

The meridional velocity component, plotted in Fig. 3b, shows almost zero velocity with no variation with height in the interior of the fluid for small enough Ekman number but strong velocities in the Ekman layers. Again, the influence of the Ekman number is mostly felt in the Ekman layers alone.

The temperature field is shown in Figs. 3c and 3d for two different vertical temperature differences and for typical values of the Prandtl and Rossby numbers. These figures clearly show that the increase in the temperature with height is almost linear in the interior of the fluid regardless of the Ekman number, a pattern which is quite similar to the zonal velocity field. However, two strong thermal layers are evident very close to the boundary plates. Again, the effect of the Ekman number is significant only in the thermal layers. Comparing Figs. 3c and 3d, it is seen that an increase in the value of $\Delta T$ results in higher values of the temperature gradients, $dT/dz$, in the interior,

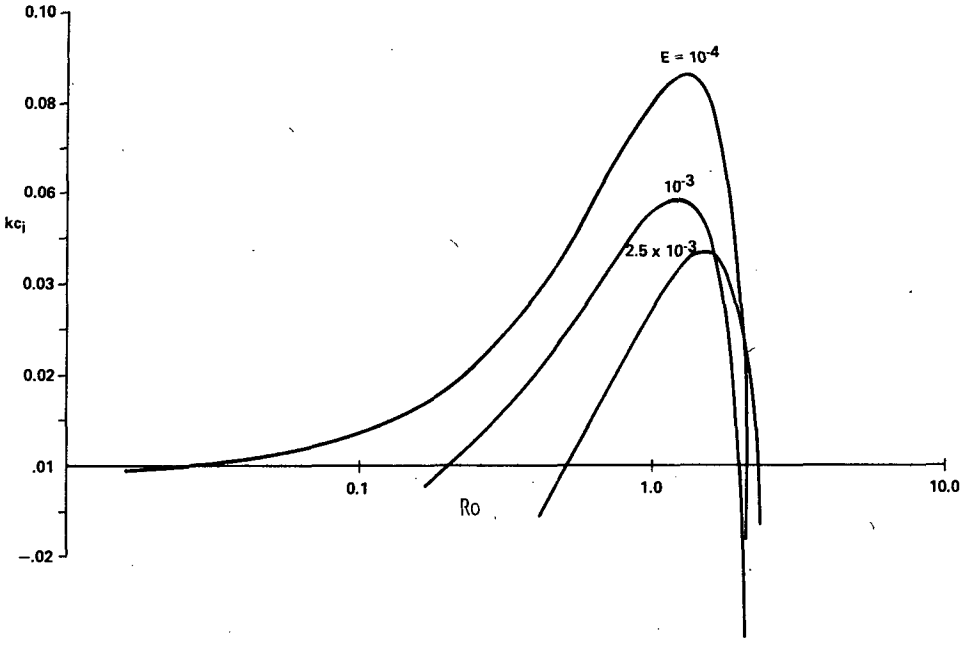


FIG. 4. Growth rates $kc_i$ as function of the Rossby number Ro at $\Delta T = 10$, $\sigma = 1$, $k = 1$ and $l = 0$ for three values of the Ekman number E.

as is shown in Fig. 3e. Note that in almost all of the cases shown the wall thermal layers are unstably stratified, while the interior fluid is stably stratified.

It can be concluded from Fig. 3 that although the velocity and temperature fields show large variations and have large gradients in the Ekman layers, the behavior in the interior of the fluid is almost independent of the Ekman number for small enough Ekman numbers, i.e., $E \ll 1$. These results show that to a substantial accuracy the interior zonal velocity and the temperature vary linearly with height, while the meridional velocity is zero for very small Ekman numbers. This fact then points to the validity of the basic state assumption of Barcilon (1964) and others in their baroclinic instability studies of quasi-geostrophic flows. Nevertheless, it should be emphasized that the departure of the velocity and temperature field from this functional behavior near the plates is very strong.

### b. *Stability results*

It can be easily seen by inspecting Eqs. (18)–(20), governing the two-dimensional perturbation functions, that the eigenvalue problem specified by these equations is a function of several parameters. The stability or instability of the basic state is greatly influenced by a variation of any one of these parameters. Hence, for a comprehensive stability analysis, the variation of $c$ with respect to all of the governing parameters must be investigated. However, due to the large number of these parameters, such a task is beyond the scope of the present discussion, although it is possible, in principle at least, to explore this question fully with the method of solution discussed earlier. In this section, only the most significant features of the stability problem will be discussed.

The stability problem as given by Eqs. (18)–(20) may be expressed in the following functional form:

$$c = F(k, \text{Ro}, \text{E}, \sigma, \Delta T). \tag{27}$$

We proceed, as is commonly done in stability analyses, to look for changes in $c_i$ while keeping all but one of the parameters on the right-hand side of (27) constant and varying the remaining parameter. Note that the specification of the physical parameters Ro, E, $\sigma$ and $\Delta T$, completely defines the basic state.

Fig. 4 shows typical growth rates as a function of the Rossby number for three values of the Ekman number. These growth rates are for a zonal wavenumber $k$ of 1 with an imposed temperature difference $\Delta T$ of 10. We note that in all of the cases discussed below and unless otherwise stated, the meridional wavenumber $l$ is always zero. It can be seen from this figure that the growth rates are typical of the classical baroclinic waves in that they increase with decreasing Ekman numbers. Also, the figure shows clearly the transition at all Ekman numbers, from the stable to the unstable regime at low Rossby numbers and the reverse transition from the unstable to the stable regime at higher Rossby numbers. It can also be seen that the Rossby numbers at which the

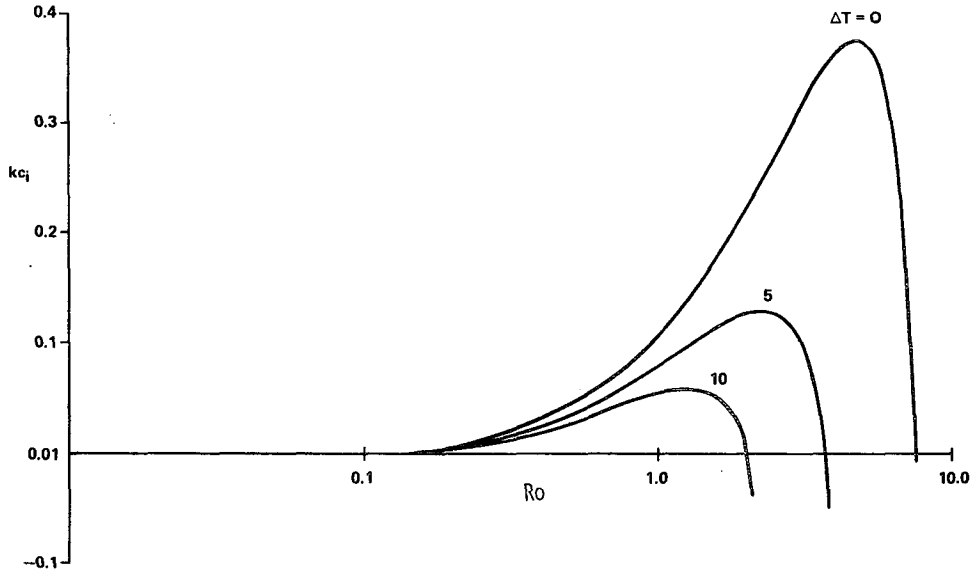


FIG. 5. Growth rates $kc_i$ as function of the Rossby number Ro at E = $10^{-3}$, $k = 1$, $\sigma = 1$, $l = 0$ for three values of the stratification parameter $\Delta T$.

maximum growth rates occur increase with increasing Ekman numbers. Note that the phase speeds $c_r$ are not listed for all of the growth rates shown. This is due to the fact that the analysis shows that both the stable and the unstable waves propagate with the mid-channel velocity; i.e., $c_r$ was found to be zero for all of the values of $c_i$ shown. This means that the unstable waves are stationary with respect to the rotating reference frame. Incidentally, this is also the speed of the propagation of the neutral waves (waves with $c_i = 0$), indicating that the principle of exchange of stability holds for this problem. Henceforth, all of the phase speeds are to be taken as zero unless otherwise indicated.

Since in Fig. 4 the results are given for a single value of $\Delta T$, Fig. 5 shows the influence of the imposed vertical stratification, $\Delta T$, on the growth rates for one value of the Ekman number. Again, in this figure the zonal wavenumber is 1. It is observed that for the unstable waves the growth rates diminish with increasing $\Delta T$. This fact is not surprising since an increase in $\Delta T$ leads to a more stable vertical stratification in the interior of the fluid for the basic state. This may be easily checked by inspecting expression (11) for the solution of the temperature field for the basic state, from which $dT/dz$ for the interior fluid (excluding the thermal layers) may be shown to be of the form

$$dT/dz\big|_{z=0} = \Delta T + \tfrac{1}{4}\mathrm{Ro}\,\sigma, \qquad (28)$$

where $df/dz \to 0$ as $z \to 0$, indicating the obvious relation between the two. Fig. 5 also shows a shift in the maximum growth rates to lower Rossby numbers with increases in $\Delta T$. This decrease in the Rossby number is also accompanied by a decrease in the range of the Rossby number over which the waves are unstable. The conclusion from this figure is that an increase in the stable stratification of the basic state is always accompanied by a decrease in the parameter range for instability with a diminished growth rate.

This last observation is clearly demonstrated in Fig. 6 which shows neutral stability curves (curves with locus of $c_i = 0$), in the Rossby-Taylor number plane for three different values of $\Delta T$. The Taylor number Ta is defined here by: $\mathrm{Ta} = \mathrm{E}^{-2}$. In this

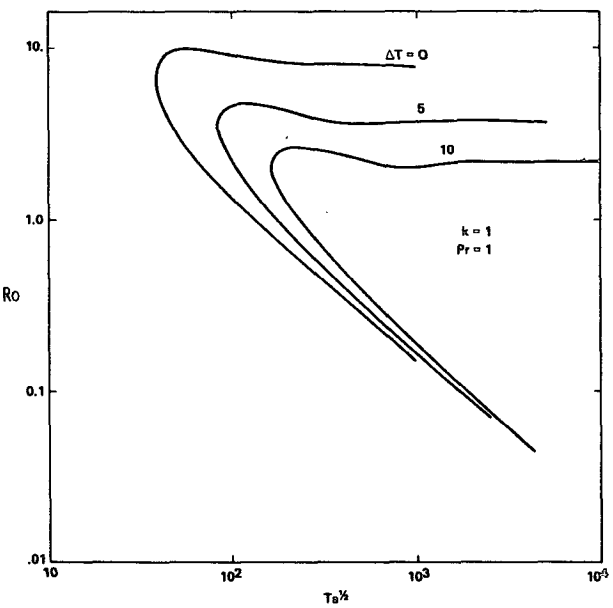


FIG. 6. Neutral stability curves at $\sigma = 1$, $k = 1$ and $l = 0$ for three values of the stratification parameter $\Delta T$.

TABLE 1. Comparison of Eady's cutoff criterion and the Rossby number analysis of Fig. 6.

| $\Delta T$ | $\sigma$ | $k$ | Eady's cutoff criterion | $Ro_\infty$ |
|---|---|---|---|---|
| 0 | 1 | 1 | 7.52 | 9.60 |
| 5 | 1 | 1 | 3.86 | 3.76 |
| 10 | 1 | 1 | 2.18 | 2.16 |
| 0 | 5 | 1 | 4.29 | 4.21 |
| 0 | 10 | 1 | 3.04 | 2.99 |
| 10 | 1 | 2 | 0.57 | 0.56 |
| 10 | 1 | 3 | 0.25 | 0.25 |
| 5 | 1 | 2 | 1.09 | 0.99 |
| 5 | 1 | 3 | 0.50 | 0.49 |

figure, as in the next several, the neutral curves separate regions of stable perturbations, which always lie to the left of the curve, from regions of unstable perturbations lying to the right of each curve. The figure shows clearly the decrease in the (Ro-Ta) plane of the range of unstable perturbations with increase in $\Delta T$. Note the qualitative similarity of these curves with the regime diagrams obtained from quasi-geostrophic models and also with the experimental annulus flow curves (e.g., Fig. 1). All of these curves possess a knee to the left of which the flow is stable regardless of the Rossby number. However, as the Ekman number is decreased, larger segments of the Rossby number region begin to emerge over which some waves become unstable. The stability results depicted by these curves may be verified by comparing the asymptotic limit of each curve with the inviscid large, Rossby number criterion of Eady (1949). This criterion written in terms of the nondimensionalizations of Section 2, states that in the limit as $E \to 0$, the Rossby number for the unstable waves is bounded from above by

$$23.04(k^2 + l^2)^{-1}(dT/dz)^{-1}.$$

Table 1 gives the values calculated for this criterion together with the values obtained from the stability analysis for the curves shown in Fig. 6. The excellent agreement for the cases of $\Delta T = 5$ and 10 is noted. However, for the case of $\Delta T = 0$ and $\sigma = 1$, the disagreement is ~20%. This discrepancy may be attributed to the fact that the maximum value of the Richardson number for this case is very close to the lower limit at which the regular baroclinic modes are dominating (see Stone, 1966) and hence the inviscid cutoff criterion is not accurate.

Figs. 7a and 7b show typical neutral stability curves with three different zonal wave numbers for two values of the imposed vertical stratification parameter $\Delta T$. It may be seen that as the wavenumber increases, the region of the unstable waves shifts to lower Rossby numbers and to lower Ekman numbers. Thus, waves with longer wavelengths are more unstable than those with shorter wavelengths. Also, it may be seen that the longer the wavelengths are, the larger is the region of instability in the regime diagrams. Again, the close similarity between these curves and the stability curves of Barocilon should be noted. The Eady cutoff criterion for the upper branches for the cases shown is in close agreement with those calculated for the inviscid limit as shown in Table 1. It appears, however, that the envelope of the individual curves is smoother than those calculated from geostrophic models (see Barcilon, 1964).

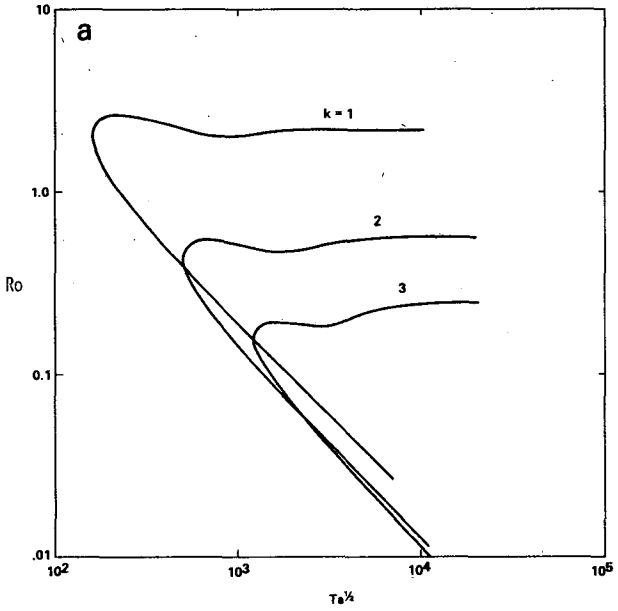


FIG. 7a. Neutral stability curves at $\Delta T = 5$, $\sigma = 1$ and $l = 0$ for $k = 1$, 2 and 3.

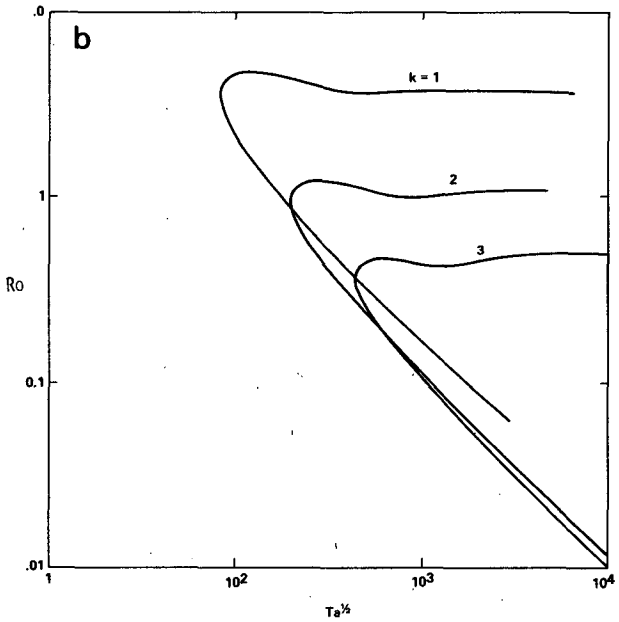


FIG. 7b. As in Fig. 7a with $\Delta T = 10$.

The influence of the Prandtl number $\sigma$ on the neutral stability curves is shown in Fig. 8 for three typical values of $\sigma$. It can be seen that an increase in the Prandtl number, in general, shifts the curves to lower Rossby numbers and to slightly smaller values of the Ekman number. Since the asymptotic limit of the upper branches of these curves seems to be in close agreement with the Eady cutoff criterion, it may be concluded that the influence of the Prandtl number is essentially felt as a modification of the basic state for vanishingly small Ekman numbers.

It is instructive at this point to digress a little and present a comparison between the present model and that of Barcilon (1964). A few words of caution are necessary. First, since basically the two models have a similar structure in the interior, especially for small Ekman numbers and large $\Delta T$, it is reasonable to expect a close agreement between the two. On the other hand, since the two differ significantly near the plates, identical results should not be expected. Furthermore, a comparison of the results is complicated by the fact that there is no direct equivalence between the two models for one of the fundamental parameters. Barcilon (1964) bases his theory and results on the parameter $\epsilon$, which is defined as $\epsilon = \Delta T_H/\Delta T_V$ and is taken to be a prescribed constant. In the present work, however, the closest approximation to $\epsilon$ may be obtained by considering the ratio of the horizontal to the vertical temperature gradients, i.e., $\gamma(dT/dz)^{-1}$. Since $dT/dz$ for this model is a constant only in the vicinity of $z = 0$, its value at mid-channel height will be considered as a representative value. Thus, for the sake of comparison, $\epsilon$ is approximated by the nondimensional form

$$\epsilon \sim (dT/dz\,|_{z=0})^{-1} = (\Delta T + \tfrac{1}{4}\mathrm{Ro}\,\sigma)^{-1}. \quad (29)$$

If the neutral curves are to be compared, as is done below, then $dT/dz$ is a function of the Rossby number as well for fixed values of $\Delta T$ and $\sigma$. This functional dependence on Ro may be minimized by taking $\Delta T$ large enough. Thus, considering, for instance, $\Delta T = 5$ and $\sigma = 1$ leads to $0.169 \leq (dT/dz\,|_{z=0})^{-1} \leq 0.20$ in the unstable wave region of regime diagram.

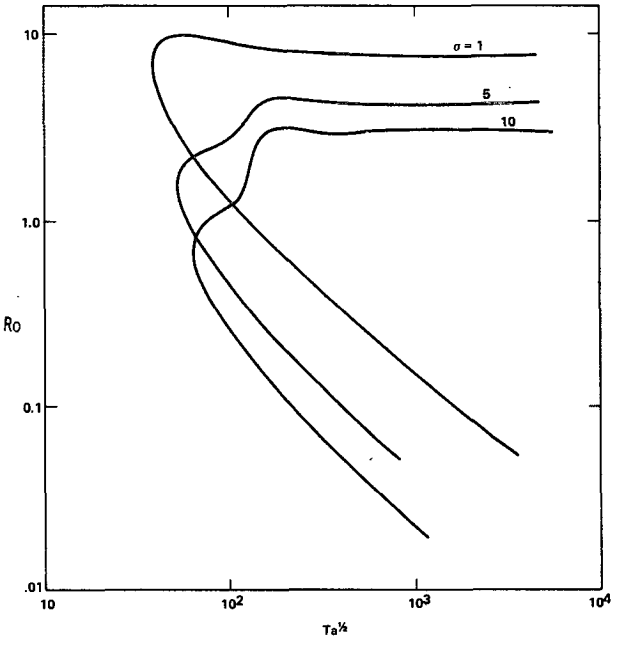


FIG. 8. Neutral stability curves at $\Delta T = 0$, $k = 1$, $l = 0$ for Prandtl numbers, $\sigma = 1$, 5 and 10.

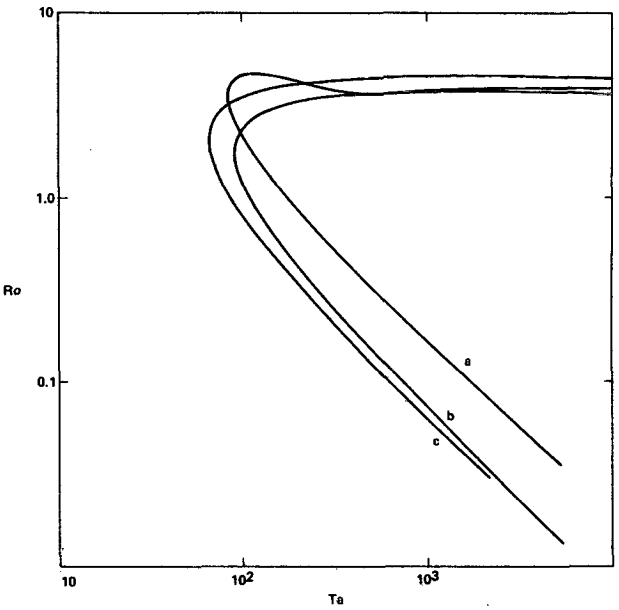


FIG. 9. Neutral stability curves at (a) present model with $\Delta T = 5$, $\sigma = 1$, $k = 1$ and $l = 0$; (b) according to Eq. (30) from Barcilon (1964) with $k = 1$, $l = 0$, and $\epsilon = 0.169$; (c) as in Fig. 9b except with $\epsilon = 0.20$.

Fig. 9 shows neutral stability curves in the (Ro-Ta) number plane as calculated from Barcilon's model for $\epsilon = 0.169$ and 0.20 and as calculated from the present model for $\Delta T = 5$ and $\sigma = 1$. In both models $k$ and $l$ were set equal to 1 and 0, respectively. The curves $b$ and $c$ were calculated from the dispersion relation of Barcilon (1964) which, when written in terms of the nondimensionalization used in Section 2, takes the form

$$c^2 - (1 - 2i\coth\kappa)c + (1/\kappa - i\delta)\coth\kappa - (1/\kappa^2 + \delta^2) = 0, \quad (30)$$

where

$$\delta^2 = \mathrm{E}/(\mathrm{Ro}\,\epsilon\kappa^2)$$

$$\kappa^2 = \mathrm{Ro}(k^2 + l^2)/4\epsilon$$

It can be seen from Fig. 9 that the agreement between the two models for the upper branch of the neutral curves $a$ and $b$ is very good as $\mathrm{E} \to 0$. This

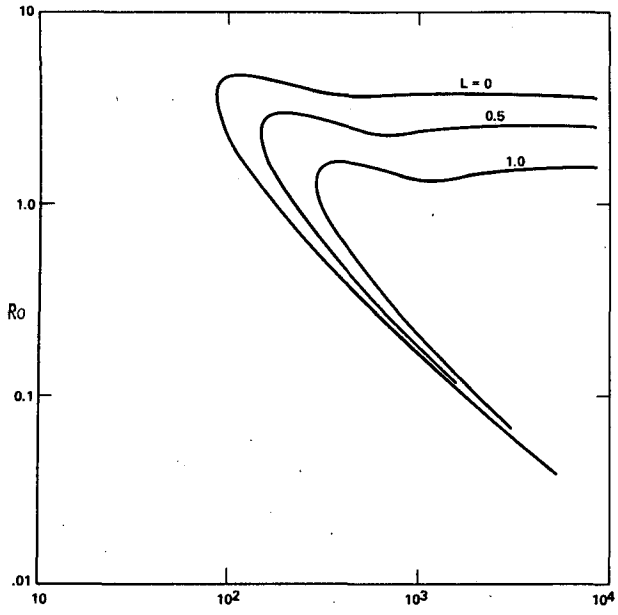


FIG. 10. Neutral stability curves at $\Delta T = 5$, $k = 1$, $\sigma = 1$ and $l = 0$, 0.5 and 1.0.

fact is to be expected since both models should recover the Eady short-wave cutoff criterion as E $\rightarrow$ 0. However, the difference between the two is significant for the upper branch at large Ekman numbers and the whole of the lower branch. The disagreement at larger Ekman numbers is to be expected since the departure from the linear velocity and temperature profiles for the basic state of the present model is increased with increased Ekman numbers, while in Barcilon's model no such deviation of the basic state is accounted for. The curve $c$ for $\epsilon = 0.2$ shows a better agreement between the two near the knee but gives larger departures for both branches of the curve. Thus, it may be concluded from this figure that the theory of Barcilon is sufficient to give good results for small Ekman numbers.

Returning to the present model, Fig. 10 shows neutral stability curves for three values of the meridional wavenumber $l$ with $k = 1$. These curves were obtained by the solution of the three-dimensional perturbation equations (23)–(26). It can be seen that increasing $l$ from zero results consistently in smaller instability regions in the regime diagrams. This result together with the fact that the growth rates also are decreased with increasing $l$, for the same values of the rest of the parameters, leads to the obvious conclusion that the purely two-dimensional perturbations are the most unstable ones. Again, we would like to emphasize that we are not considering the symmetric baroclinic instability case.

Figs. 11a and 11b show typical eigenfunctions for E = $2.5 \times 10^{-3}$, $k = 1$, $\sigma = 1$, and $\Delta T = 10$ at maximum growth rates for these values of the parameters. Fig. 11a shows the amplitudes of the eigenfunctions for the vertical velocity $w$, the temperature $\theta$ and the pressure $p$, respectively. It is seen that the amplitudes of these functions are symmetric with respect to the mid-channel height, $z = 0$. The amplitude of the normal velocity perturbations increases monotonically from zero at $z = -\frac{1}{2}$ to a maximum value at $z = 0$. Similarly, the amplitude of the pressure perturbation decreases monotonically from a maximum at $z = -\frac{1}{2}$ to a minimum at $z = 0$. The amplitude of the temperature perturbation, however, increases from zero at $z = -\frac{1}{2}$ to a maximum at $z = -0.3$ and then decreases to a relative minimum at $z = 0$. The behavior of the amplitudes of these functions appears to be qualitatively similar to those calculated from the inviscid theory (see Eady, 1949), except in the vicinity of the plates where the viscous and thermal effects are present. The negative phases of these perturbation functions are shown in Fig. 11b, for the vertical velocity, temperature and pressure, respectively. The phases of the velocity and temperature perturbations appear, at first sight, somewhat different from those for the inviscid case. Observe, however, that in the vicinity of the mid-channel height, the phases of both the temperature and the velocity perturbations are similar to the inviscid case in that the negative phase for the temperature slightly increases with height, while for the velocity it decreases with height. This limited similarity may be due to the fact that for this value of the Ekman number, the linear portion of the basic state profiles is small and confined to the mid-channel position (see Fig. 3). The phase of the pressure perturbation, on the other hand, seems to correspond with the inviscid theory in that the negative phase decreases monotonically with height. However, the difference in the pressure phase seems to be approximately $2\pi/3$, while it is exactly $\pi/2$ for the inviscid case.

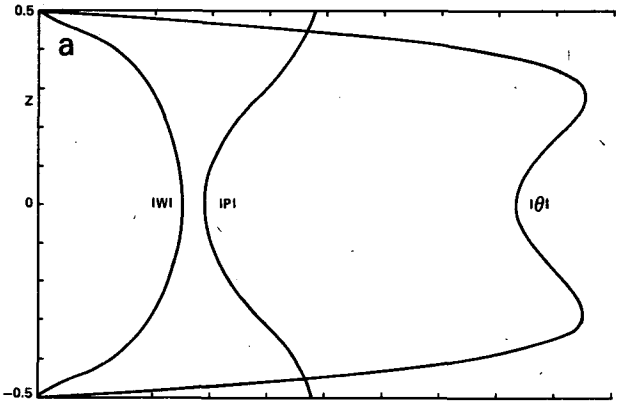


FIG. 11a. The amplitude of the eigenfunctions $w$, $\theta$ and $p$ for E = $2.5 \times 10^{-3}$, $\Delta T = 10$, $k = 1$, $l = 0$, $\sigma = 1$, Ro = 1.55 and $c_i = 0.0471$.

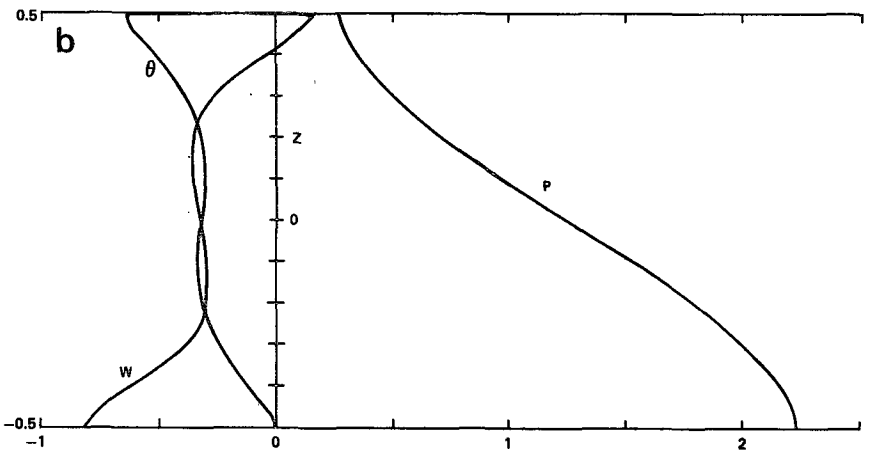


FIG. 11b. The negative phases (rad) of the eigenfunctions, $w$, $\theta$ and $p$ for the same values of the parameters as in Fig. 11a.

## 6. Concluding remarks

We have shown that for a rotating, stratified, two-dimensional flow between two parallel horizontal plates which are subjected to a horizontal temperature gradient, there exists a simple, closed form solution for the stationary basic state. This solution identifies the strong Ekman and thermal layers adjacent to the plates with velocity and temperature fields in the interior strongly dependent on the Ekman, Rossby and Prandtl numbers. Also, we have shown that this solution is unstable with respect to infinitesimal perturbations which are in the form of purely zonal waves, for small enough Ekman numbers. We have established the instability criteria as a function of the controlling parameters for a relatively few important cases. The stability analysis of the present model confirms the results obtained in the past for a quasi-geostrophic flow with a postulated simple basic state. The influence of the Prandtl number and the imposed vertical stratification on the stability problem are new results for baroclinic instability studies.

*Acknowledgment.* The work reported here was supported by NASA, Office of Space and Terrestrial Applications, under Contract NAS8-33386, whose financial support is greatly appreciated.

## REFERENCES

Barcilon, V., 1964: Role of Ekman layers in the stability of the symmetric regime obtained in a rotating annulus. *J. Atmos. Sci.*, **21**, 291–299.

Charney, J. G., 1947: The dynamics of long waves in a baroclinic westerly current. *J. Meteor.*, **4**, 135–162.

Conte, S. D., 1966: The numerical solution of linear boundary value problems. *S.I.A.M. Rev.*, **8**, 309–320.

Davey, A., 1978: Numerical methods for the solution of linear differential eigenvalue problems. *Rotating Fluids in Geophysics*, P. H. Roberts and A. M. Soward, Eds., Academic Press, 551 pp.

Eady, E. T., 1949: Long waves and cyclone waves. *Tellus*, **1**, 35–52.

Fehlberg, E., 1969: Klassische Runge-Kutta-Formeln funafter und siebenter ordnung mit schrittweiten-kontrolle. *Computing*, **4**, 93–106.

Fowlis, W. W., and R. Hide, 1965: Thermal convection in a rotating annulus of liquid effects of viscosity on the transition between axisymmetric and non-axisymmetric flow regimes. *J. Atmos. Sci.*, **22**, 541–558.

Fultz, D., 1953: A survey of certain thermally and mechanically driven fluid systems of meteorological interest. *Fluid Models in Geophysics, Proc. First Symp. Use of Models in Geophysical Fluid Dynamics*, Baltimore, 27–63.

——, R. R. Long, G. V. Owens, W. Bohan, R. Kaylor and J. Weil, 1959: *Studies of Thermal Convection in a Rotating Cylinder with Some Implications for Large-Scale Atmospheric Motions. Meteor. Monogr.*, No. 21, Amer. Meteor. Soc., 104 pp.

Geisler, J. E., and W. W. Fowlis, 1979: Theoretical regime diagrams for thermally driven flows in a beta-plane channel. *J. Atmos. Sci.*, **36**, 1530–1541.

Greenspan, H. P., 1968: *The Theory of Rotating Fluids*. Cambridge University Press, 328 pp.

Hart, J. E., 1972: Stability of thin non-rotating Hadley circulations. *J. Atmos. Sci.*, **29**, 687–697.

Hide, R., 1958: An experimental study of thermal convection in a rotating liquid. *Phil. Trans. Roy. Soc. London*, **A250**, 441–478.

Kaiser, J. A. C., 1970: Rotating deep annulus convection. Part 2. Wave instabilities, vertical stratification, and associated theories. *Tellus*, **22**, 275–287.

Lorenz, E. N., 1962: Simplified dynamic equations applied to the rotating-basin experiments. *J. Atmos. Sci.*, **19**, 39–51.

O'Neil, E. J., 1969: The stability of flows in a differentially heated rotating system with rigid bottom and free top. *Stud. Appl. Math.*, **48**, 222–256.

Pedlosky, J., 1979: *Geophysical Fluid Dynamics*. Springer-Verlag, 624 pp.

Stone, P. H., 1966: On non-geostrophic baroclinic stability. *J. Atmos. Sci.*, **23**, 390–400.

Williams, G. P., 1967: Thermal convection in a rotating fluid annulus: Part 1. The basic axisymmetric flow. *J. Atmos. Sci.*, **24**, 144–161.